THE EFFECT OF EXPLOSIVE DETONATION CHARACTERISTICS ON SHAPED CHARGE PERFORMANCE

Julius Simon

Ballistic Research Laboratories
Aberdeen Proving Ground, Maryland

1974

THE EFFECT OF EXPLOSIVE DETONATION CHARACTERISTICS ON SHAPED CHARGE PERFORMANCE

JULIUS SIMON
BALLISTIC RESEARCH LABORATORIES
ABERDEEN PROVING GROUND, MARYLAND

I. INTRODUCTION

The jet formation caused by the collapse of a shaped charge liner is dependent upon the pressure delivered to the liner wall by the detonating explosive. As a shaped charge liner is collapsed axisymmetrically to the charge axis by a detonation wave to form a jet and a slug, the liner material experiences plastic deformation at exceedingly high strain rates (1). If the jet is presumed to form simultaneously on the axis, and then stretch uniformly, a one dimensional approximation shows that strain rates characteristic of this process are 10^4/second. It is assumed that the jet is a ductile material which remains continuous during stretching.

It is apparent also that the initial jet formation occurs under conditions of relatively high pressures whereas the later phases of jet flight and stretching occur essentially under ambient pressure. Therefore, it is clear that the interesting plastic deformation occurs in two distinct stages.

The purpose of this study was to determine the influence of explosive filler on shaped charge warhead performance (2). To minimize variations due to hardware or explosive loading, only high quality metal components and explosives with established loading procedures were used in this study.

Ten explosive fills, loaded into the BRL, 81.3mm, precision charge, have been evaluated on the basis of warhead performance and implications regarding fundamental jet properties. Multiple flash radiography of the free flight jet and penetration performance of the shaped charge warhead against armor were used to evaluate the performance.

Additionally, the BRL Analytic Shaped Charge (BASC) code has been extensively employed in the interpretation of results (3). BASC was derived from the model of Defourneaux (4) and substantially modified and extended to include the explosive-metal coupling as described by Defourneaux, the non-steady hydrodynamic jet formation theory (5), and a BRL developed penetration theory, Reference 6.

Two conclusions have been derived from this work; viz. a.) warhead performance increases with increasing explosive energy and b.) jet elongation increases with explosive energy. It is argued that the latter implies jet strain to fracture increases with strain r-

II. EXPERIMENTAL FIRINGS

The liners and bodies used conform to the BRL precision shaped charge shown in Figure 1. With a warhead design of this quality, imperfections attributable directly to assembled parts are reduced to a minimum; therefore, the results should reflect the properties of the explosive fill.

The explosives loaded into the test assemblies are listed in Table I. Tabulated are explosive composition, Chapman-Jouguet (C-J) detonation pressure, detonation rate, measured tip velocity and loading facility. For later application of the BASC code, the detonation rate is compared to the measured jet tip velocity in Table I.

Flash radiographs of the shaped charge jets in free flight were obtained. Jet particle velocities, break-up times and jet lengths were measured as described in reference (2). The precision of the charge was subjectively appraised by radiographic observation of the alignment of jet particles on the charge axis, and the physical break-up of the particulated jet. Penetration and hole volume were measured in stacked plates (76.2mm thick x 152.4mm x 152.4mm) of armor (280 BHN) for each explosive fill at two cone diameters standoff (162.6mm). Hole volumes and profiles were obtained by volumetric titration.

III. EXPERIMENTAL DATA

A. Flash Radiography

The quantities measured from radiographs were: jet tip velocity, velocity of 31st particle, the velocity difference between the 1st and 31st particles, jet break-up time, the length of thirty particles from the tip, length of particles between the thirtieth

and the particle with a velocity of 0.28 cm/μsec (the velocity below which significant penetration does not occur (7)), the sum of the total jet length, number of jet particles, and average jet particle length. A summary of measurements appears in Table II.

Jet length as a function of jet tip velocity is plotted in Figure 2. The average total length of the first thirty particles is 36.43 cm. The total length of solid jet involved in the penetration process of steel (jet particle velocities > 0.28 cm/μsec) is represented by the diagonal line, and is shown to increase with explosive energy.

The actual radiographs of jets (at a nominal x-ray delay time of 206 μsec after initiation) from six selected explosives are shown in Figure 3. Jet tip velocity decreases from left to right. The jet tip velocity is shown to decrease with decreasing explosive energy. The two diagonal lines indicate the approximate space orientation of the first and thirty-first particles. The sum of the lengths of the particles bounded by the diagonals are essentially equal. It can be seen in Figure 2 and Table II that there is a monotonic increase in jet length available for additional penetration when the explosive energy is increased.

B. Jet Break-up Time (t_1)

The most difficult jet parameter to estimate is jet break-up time. It is assumed that jet fractures occur simultaneously. By measuring the lengths of thirty jet particles on the radiograph, an estimate of the break-up time can be made by equation:

$$t_1 = \frac{\ell}{\Delta v}$$

where ℓ = length of thirty particles and Δv is the difference in jet velocity between tip and thirty-first particle. The average jet break-up time for all explosives is estimated at 115.9 μsec. Listed in Table II is the average break-up time for each explosive. With the exception of the ECX-LLL explosive, experimental measurements of t_1, for all the explosives, had individual values which were included in a range of break-up time of 115.9 ± 3% (119.4 - 112.4 μsec). This justified the assumption of a constant breakup time for all explosives.

C. Penetration and Hole Volume Data

Penetration and hole volume data are summarized in Table III. Tabulated are the experimental averages, maximum values, and theoretical penetration with an assumed constant t_1. Penetration and

hole volume are seen to increase with increasing explosive potential.

D. Comparison of Confinement and Explosive Energy

Penetration performance data (8) is available for cylindrical, steel and aluminum cased, composition B loaded warheads. The warhead contains a 83.8mm, 2.5% wall, 42° copper liner. The penetration depth into 300 BHN armor at 2 C.D. standoff is 430mm for the confined charge and 372mm for the unconfined charge.

Data from the present experiments show that for warheads loaded with PBXW-111 the penetration is 424 mm; while for warheads loaded with composition B, the penetration is 389 mm. The effect of increased confinement and increased explosive energy on performance are seen to be similar. Such confinement effects have been verified in previous experiments using radioactive tracer techniques (9) and by measurements on free flight jet radiographs (10).

IV. DATA ANALYSIS

From the radiographs it was determined that the difference in velocity of the jet tip and the thirty-first particle is approximately independent of explosive fill (i.e. Table II). However, computing the jet velocities employing the BASC code, one notes that the portions of the liners contributing to these jet segments vary with the explosive fill. Figure 4, which depicts the correspondence between jet velocity and original liner axial coordinate, demonstrates this point. So, for instance, we see that for the ECX explosive the 31 particles originate from the relative liner zone between 0.13 and 0.49 from the cone apex and for TNT from 0.13 to 0.61.

Total penetration, at two cone diameters standoff, shows a monotonic increase with increasing explosive potential. A computation of the penetration is consistent with observation. Assuming, no penetration occurs for jet elements with velocities less than 0.28 cm/μsec, one again can infer computationally that different liner elements for different explosives participate in penetration. Figure 5, which depicts penetration as a function of liner position, exposes this point. From this computation it appears that the higher the explosive potential the larger the liner zone entering the penetration process.

A. Jet Velocity

The change in jet velocity between the jet tip and the thirty-first particle is approximately the same for all explosives

(Figure 4 and Table II). However, the jet velocity decreases and the reference zone of the thirty-first element increases toward the base with decreasing energy explosive composition. As shown in Figure 4 and 5, the jet "cutoff" particle comes from the liner section closer to the base for the higher energy explosives. The total penetrating jet length produced by the most energetic explosive has the greatest total change in jet velocity.

B. Cumulative Penetration Contribution by Liner

It was noted earlier than the first thirty particles of jet were approximately the same length. Figure 5 shows that these particles provide about the same target penetration for each explosive. The liner sections contributing to this equivalent penetration are most efficient for the most energetic explosives. The greater total penetration depth for the high energy explosive is due to greater jet length and to more liner material in the base region participating in penetration. The agreement in penetration between calculation and experiment is tabulated in Table III.

C. Jet Elongation and Ductility

Employing the BASC computations and the above data, one can examine jet elongation in an approximate, one dimensional analysis. The strain at break-up is defined as:

$$\varepsilon = \frac{\Delta \ell}{\ell_o} = \frac{t_1}{t_o} - 1 \qquad (1)$$

where ℓ_o is the original length of jet on the axis when the last penetrating jet element finishes its collapse process. The increase in jet length in the time interval from initial jet formation to jet breakup is $\Delta\ell$. The jet elongation, $\Delta\ell$, is given by:

$$\Delta \ell = (V_j^{\,o} - V_j^{\,c.o.})t, \qquad (2)$$

where t is the time interval involved, $V_j^{\,o}$ the jet tip velocity, and $V_j^{\,c.o.}$ the velocity of the last penetrating jet particle. The strain rate at breakup is given by

$$\dot{\varepsilon} = \frac{d\varepsilon}{dt} \quad \frac{1}{\ell_o} \frac{d\Delta\ell}{dt} \quad \frac{V_j^{\,o} - V_j^{\,c.o.}}{\ell_o} = 1/t_o \qquad (3)$$

The quantities, ℓ_o, $\Delta\ell$, V_j^o, and $V_j^{c.o.}$ are readily obtained from the BASC computer code output. Figure 6 shows how quantities calculated from the code were used to evaluate formulas, 1 and 3 for strain and strain rate, respectively. The BASC code calculates an initial length, ℓ_o, at a time, t_o, based on the tip (V_j^o) and tail ($V_j^{c.o.}$) velocities. The computed values of ε and $\dot{\varepsilon}$ are calculated at a constant breakup time, t_1 = 115.9 μsec. The results are plotted in Figure 7 as strain vs. strain rate for each explosive fill. The strain and strain rate increase linearly with the Chapman-Jouquet pressures.

Elongation for the total penetrating jet at break-up ranged from 290 to 360%; and the strain rate ranged from 0.035 to 0.041 $(\mu sec)^{-1}$. For the first thirty particles of the jet, strain and strain rate are about 25% higher. These measurements indicate that copper exhibits a greater ductility at high strain rates. Various models for this behavior have been proposed by Chou (11) but additional verification of models are necessary.

V. CONCLUSIONS

1. For a given geometry warhead, an increase in the explosive energy causes an increase in the overall warhead penetration capability. The increased detonation rate explosives introduce higher collapse velocities, increased jet velocities, and penetrating jets with increased lengths. Additionally, the greater the explosive energy, the larger the proportion of the liner that ultimately becomes penetrating jet. These effects combine to produce longer, more massive and higher energy jets from more energetic explosive fills.

2. For a given design configuration with the same explosive composition, increasing confinement provides the same effect as a more energetic explosive fill. Both confinement and explosive energy can be used to increase kinetic energy of the jet.

3. A more energetic explosive appears to increase the jet ductility. The strain to fracture vs. average strain rate to fracture increases with explosive energy.

VI. REFERENCES

1. L. Zernow and J. Simon, "High Strain Rate Plasticity of Liner Materials and Jet Behavior", BRL Report No. 954, August 1955.

2. J. Simon and R. DiPersio, "The Evaluation of the Effect of Explosive Filler on Shaped Charge Performance and Lethality Effectiveness", BRL Report No. 1552, October 1971.

3. J. Harrison and R. DiPersio, "BASC-Ballistic Research Laboratories Analytical Shaped Charge Code Users Manual", (Report in Process of Publication), March 1974.

4. M. Defourneaux, "Hydrodynamic Theory of Shaped Charges and of Jet Penetration", Memorial De L'Artillerre Francaise, T44, 1970, 2^{e} FASC, pp. 293 - 334.

5. E. M. Pugh, R. J. Eichelberger, N. Rostoker, "Theory of Jet Formation by Charges with Lined Conical Cavities", J. Appl. Phys, Vol. 23, No. 5, May 1952, pp. 532 - 536.

6. R. DiPersio, J. Simon, A. Merendino, "Penetration of Shaped Charge Jets Into Metallic Targets, BRL Report No. 1296, September 1965.

7. J. Simon and R. DiPersio, "Experimental Verification of Standoff Effects on Shaped Charge Jet Cutoff in Solid Targets", BRLM No. 1976 May 1969.

8. Final Report, "Shaped Charge Scaling Study" Contract No. DAAD 21-68-C-0124, March 1970, Firestone Tire and Rubber Co., Akron, Ohio.

9. M. K. Gainer, "Application of Radioactive Tracers to Shaped Charge Liners to the Study of Shaped Charge Phenomena", BRL Memo Report No. 1242, January 1960.

10. J. Simon, F. E. Allison, R. DiPersio, "Penetration Capabilities of Confined and Unconfined Shaped Charges" BRL Memo No. 1471, May 1963.

11. P. C. Chou, H. S. Sidhu, R. W. Mortimer, "A Study of the Break-up of Shaped Charge Jets", DIT-125-4, April 1963, Drexel Institute of Technology, Phil., Pa., (BRL Contract DA-36-034-ORD-3672RD).

TABLE I. CANDIDATE EXPLOSIVE FILLER CHARACTERISTICS

EXPLOSIVE	COMPOSITION	ESTIMATED C-J DETONATION PRESSURE (G PA)	ESTIMATED DETONATION RATE m/sec	MEASURED*** TIP VELOCITY m/sec	LOADING FACILITY
LLL-ECX*	78HMX/22AFNOL	35.0	8800	8800	Extrusion cast LLL
PBX-W-111*	80HMX/20AFNOL	35.0	8800	8480	Vacuum cast NOL
OCTOL(75/25)**	75HMX/25TNT	32.0	8600	8460	Cast BRL
PBXW-110*	80RDX/20AFNOL	32.0	8500	8260	Cast NOL
OCTOL(70/30)**	70HMX/30TNT	31.0	8300	8070	Cast PA
COMP B**	60RDX/40TNT/1WAX	27.0	7900	7700	Cast PA
PENTOLITE*	50PETN/50TNT	23.0	7500	7420	Cast PA
AMATEX-40*	40RDX/40TNT/20AN	19.0	6900	7350	Cast PA
H-6*	45RDX/30TNT/20AL/5WAX	19.0	7400	7020	Cast NOL
TNT*	100TNT	19.0	6800	6770	Cast PA

NOTE: LLL - Lawrence Livermore Lab.
NOL - Naval Ordnance Lab.
BRL - Ballistic Research Labs.
PA - Picatinny Arsenal

* Estimates of detonation pressure and detonation rates by H. F. Eccleston, NOL.

** Estimates of detonation pressure and detonation rates by J. D. Hopper, PA.

*** Values of detonation pressure and detonation rate give relative ranking of explosive energy to be compared to the jet tip velocity.

TABLE II. SUMMARY OF RADIOGRAPHIC DATA

EXPLOSIVE	V_j^o (cm/μsec)	V_j^{31} (cm/μsec)	$(V_j^o - V_j^{31})$ (cm/μsec)	t_1 (μsec)	ΣL_1^{30} (cm)	ΣL_{31}^N (cm)	ΣL_1^N (cm)	N	$\bar{L}_N$ cm
LLL	0.88	0.59	0.29	122.4	37.3	44.3	81.6	60	1.36
PBXW-111	0.85	0.55	0.30	117.4	36.9	37.9	74.8	58	1.29
OCTOL(75/25)	0.85	0.56	0.29	122.7	36.6	39.8	76.4	58	1.32
PBXW-110	0.83	0.53	0.30	120.7	36.6	38.8	75.4	58	1.30
OCTOL(70/30)	0.81	0.52	0.29	120.6	36.5	34.0	70.5	56	1.26
COMP B	0.77	0.46	0.31	115.7	38.2	26.9	65.1	46	1.42
PENTOLITE	0.74	0.45	0.29	111.8	34.7	25.6	60.3	44	1.37
AMATEX-40	0.74	0.42	0.32	106.8	35.0	20.8	55.8	47	1.19
H-6	0.70	0.40	0.30	108.9	37.2	11.8	49.0	41	1.20
TNT	0.68	0.38	0.30	111.8	35.3	10.9	46.2	34	1.36
AVERAGE			0.30	115.9	36.43				1.31

where: V_j^o - Jet tip velocity

V_j^{31} - Jet velocity particle 31

$(V_j^o - V_j^{31})$ - Change in velocity between particle 1 and 31

t_1 - Jet break-up time

ΣL_1^{30} - Jet length 30 particles

ΣL_{31}^N - Jet length from particle 31 to last particle with velocity of 0.28 cm/μsec

ΣL_1^N - Total jet length

N - Number of jet particles to velocity of 0.28 cm/μsec

$\bar{L}_N$ - Average particle length

TABLE III. SUMMARY OF PENETRATION AND HOLE VOLUME DATA AT TWO CONE DIAMETERS STANDOFF

Armor is 280 BHN

Explosive Composition	Experimental Average		Experimental Maximum		Theoretical Penetration with Constant t_1 (mm)
	Penetration (mm)	Hole Volume (cc)	Penetration (mm)	Hole Volume (cc)	
PBXW-111 **	424.2	105.8	452.1	111.0	419.0
OCTOL (75/25)	417.0	95.7	426.7	98.5	417.9
PBXW-110(*)(**)	411.5	94.1	426.7	100.4	407.4
OCTOL (70/30)	406.4	93.8	424.2	98.8	397.2
COMP B	388.6	79.8	401.3	80.8	377.1
PENTOLITE	378.5	75.7	383.5	77.8	361.7
AMATEX-40	365.7	68.4	378.5	70.5	357.8
H-6	355.6	59.3	358.1	61.9	339.2
TNT	322.6	47.6	327.7	53.3	324.8

No penetration data for LLL-ECX. Flash radiography only.

* Metal parts assembly disturbed prior to loading

**Standardization of loading process necessary and post-curative cracking of explosive observed.

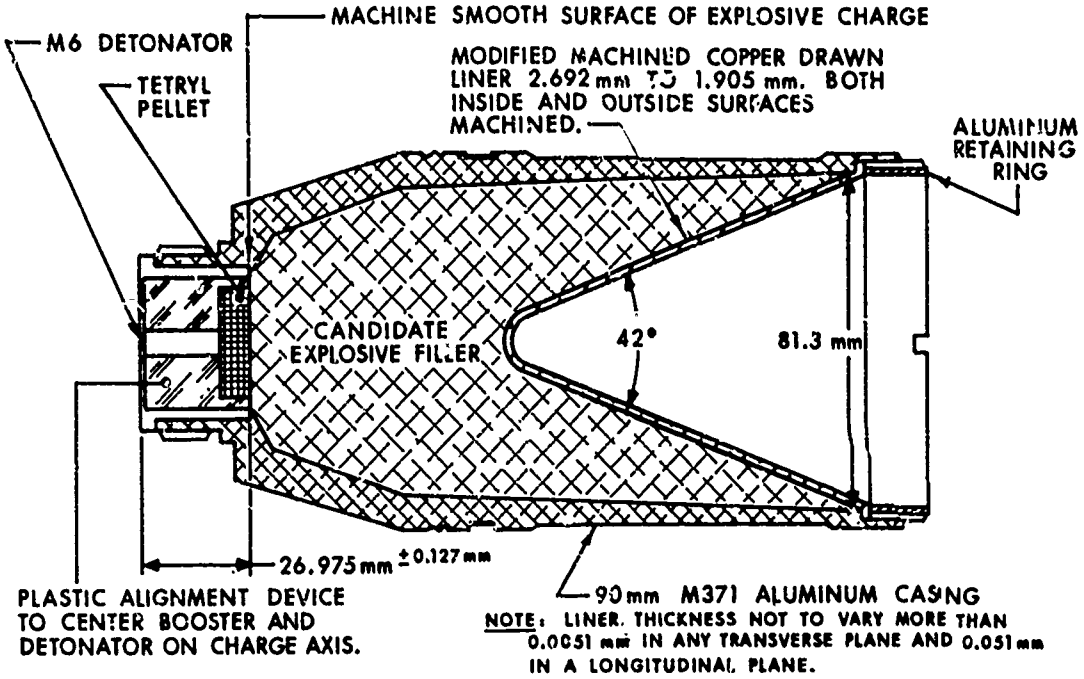

Figure 1. Sketch of 81.3 mm BRL Precision Charge.

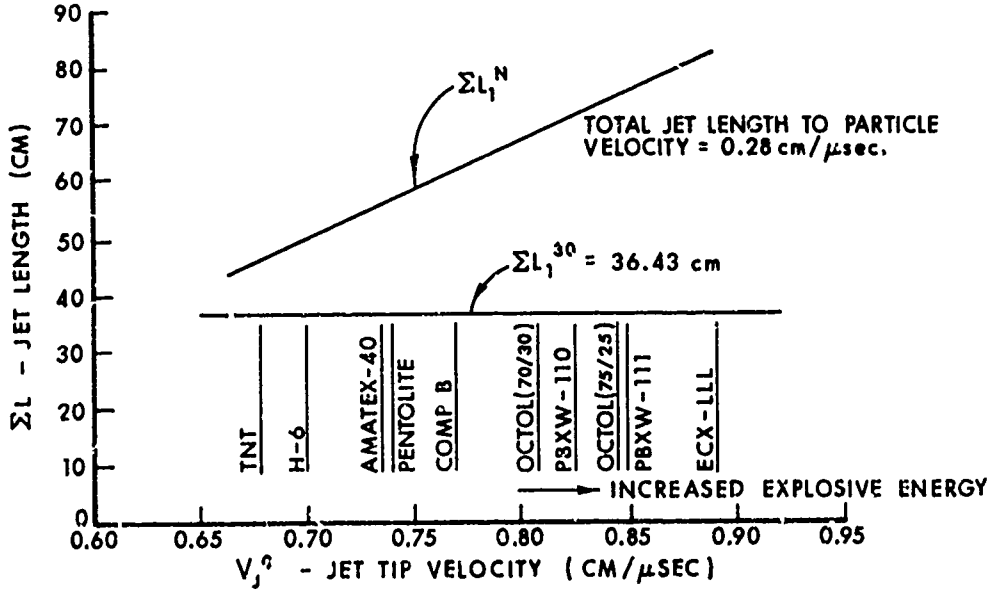

Figure 2. Estimate of Jet Length vs Jet Tip Velocity.

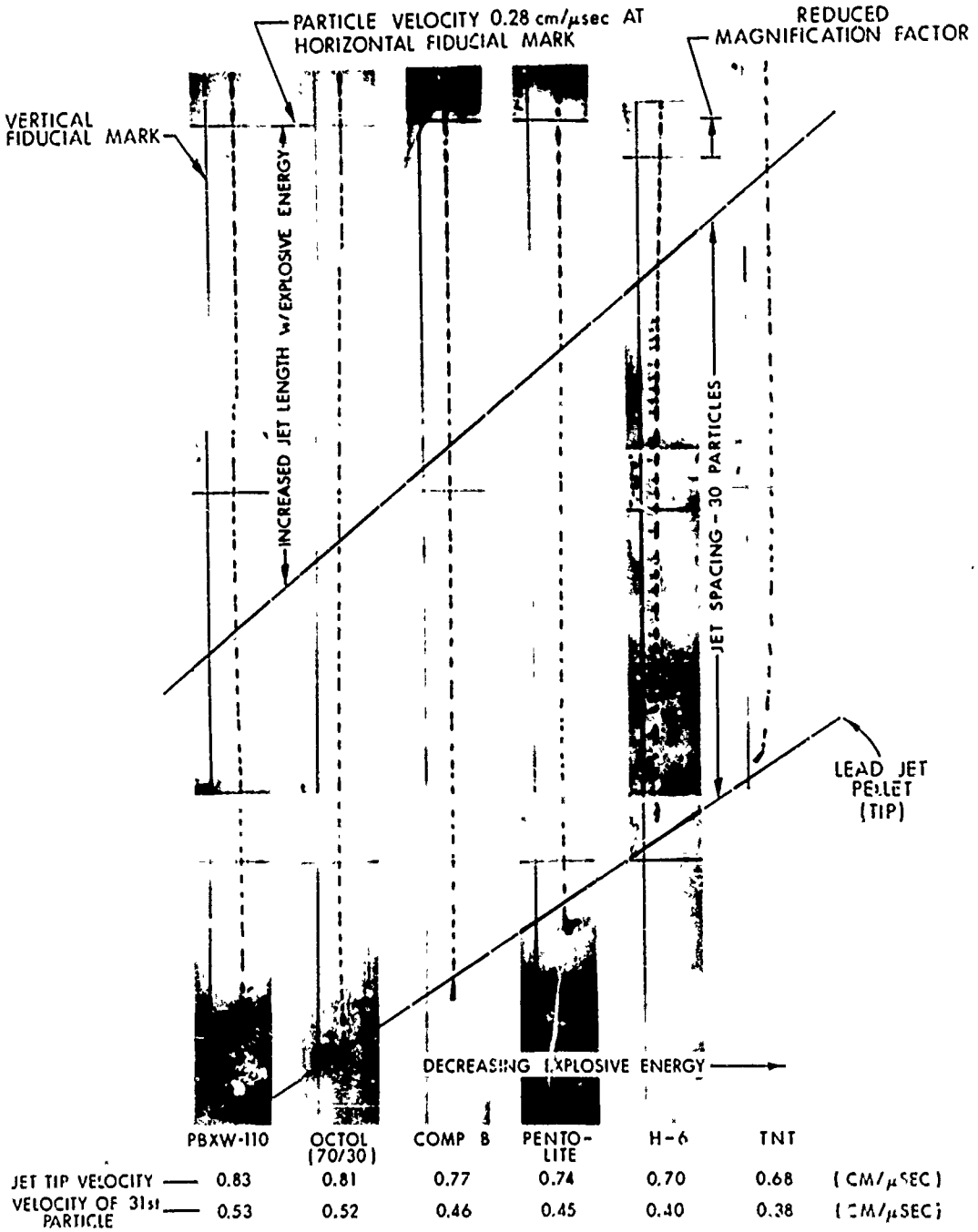

Figure 3 Comparison of Radiographs of Jets from Explosives Shown Nominal X-ray Delay Time After Charge Initiation 206.0 μsec.

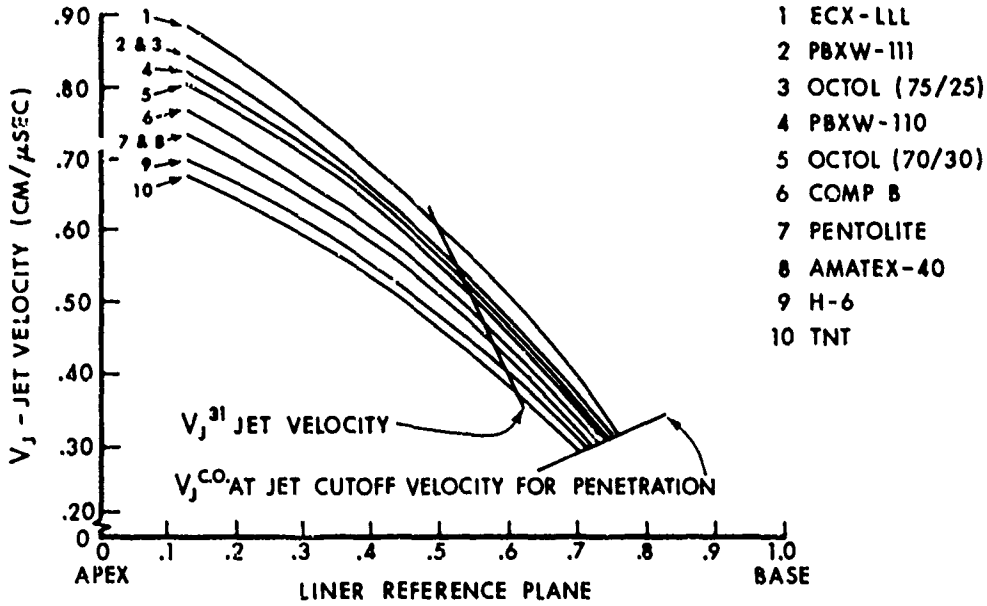

Figure 4. Jet Velocity vs Reference Plane.

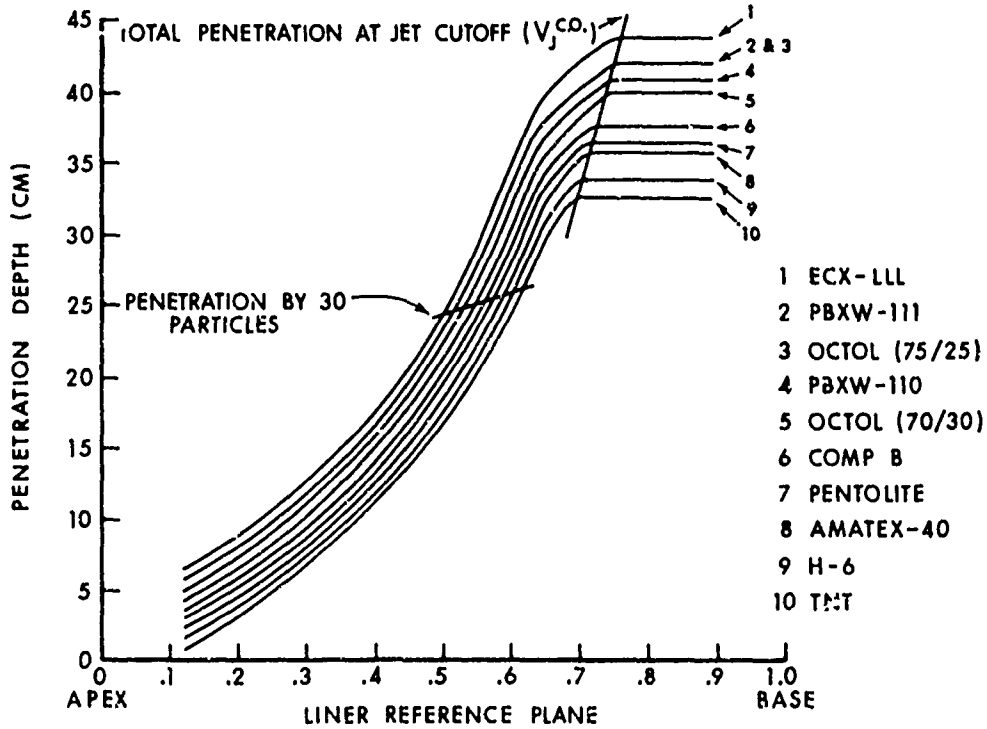

Figure 5. Penetration Depth vs Liner Reference Plane. Standoff 2 Cone Dia., Armor 280 BHN.

(1) BASC CODE CALCULATES INITIAL LENGTH BASED ON JET TIP AND JET "CUTOFF" VELOCITY.

(2) DIAGRAM JET FORMATION AND ELONGATION TO JET BREAK-UP.

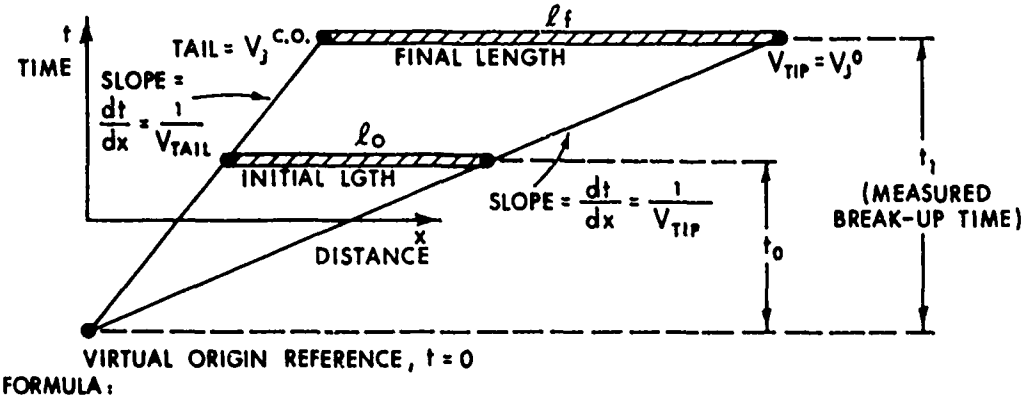

(3) FORMULA:

TIME OF INITIAL JET LENGTH TO FORM ON AXIS, $t_o = \frac{\ell_o}{V_j^0 - V_j^{c.o.}}$ (1)

STRAIN, $\epsilon = \frac{\ell_f - \ell_o}{\ell_o} = \frac{(V_j^0 - V_j^{c.o.})(t_1 - t_o)}{(V_j^0 - V_j^{c.o.})t_o} = \frac{t_1}{t_o} - 1$ (2)

STRAIN RATE, $\dot{\epsilon} = \frac{t_1 - t_o}{t_o(t_1 - t_o)} = \frac{1}{t_o}$ (3)

Figure 6. Method to Calculate Strain and Strain Rate.

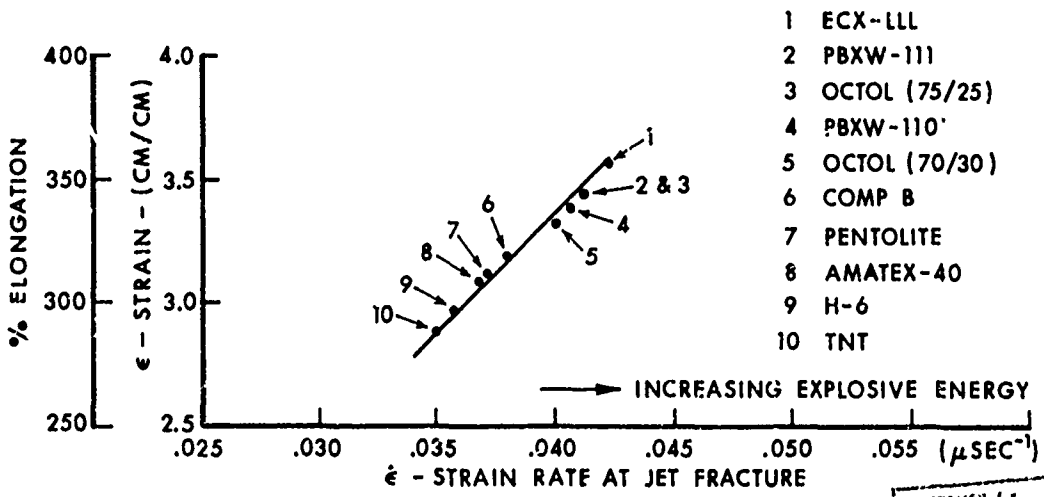

Figure 7. Total Strain vs Strain Rate for All Candidate Explosives at a Constant Break-up Time.